Electron-Beam-Stabilized Discharge in a Flowing Medium: Numerical Calculations

C. G. Parazzoli*
Northrop Research and Technology Center, Palos Verdes Peninsula, Calif.

A numerical computational method for the calculation of the bulk characteristics of an electron beam/sustainer discharge, in the presence of a flowing or stationary medium, is presented. The sustainer electric field is taken perpendicular to the flow direction, as it is commonly found in a large class of high-energy electrically pumped lasers. A detailed discussion of the underlining assumptions of the computational method is given. Typical results of the numerical calculations are presented in detail.

Introduction

IT is, at present, a commonly used technique to stabilize an electrical discharge in a large volume of gas by means of external ionization. One widely employed external source of ionization is an electron beam. This practice generally is referred to as an electron-beam-stabilized discharge. The ionizing electrons are generated in an electron gun and injected into the main body of the discharge through a thin foil, which, in general, acts also as one electrode of the discharge itself.

The externally stabilized discharge, since it first was demonstrated,[1] led naturally to the electron-beam sustainer lasers, which inlude a whole variety of laser types, such as CO, CO_2, KrF, etc. Initial investigations on the nature of an electron-beam-stabilized discharge are reported in Refs. 2 and 3. In these first investigations, the importance of the external ionization distribution in determining the electric field, current, and power distribution in the discharge was soon recognized.

Subsequent experimental observation,[4] in a supersonic CO electric discharge laser (EDL), showed that the flowing of the gas between the two electrodes could lead to nonuniform current density distributions over the cathode. It is the purpose of this paper to supply a realistic field and power distribution in a two-dimensional EDL cavity with or without a flowing medium.

Analytical Model

In our analytical model, we shall consider the two-dimensional case. A gas is flowing between two paralle electrodes (see Fig. 1) in the x direction. The high-energy ionizing electrons fo the e gun are injected through the anode foil as shown by the small arrows on the anode in Fig. 1. The e-gun foil can be taken to be coincident with the anode or to be only a portion of it. A voltage is applied between the anode and the cathode which will drive the discharge. In this paper, we shall assume steady state. It must be observed that the steady-state assumption for a discharge in a flowing medium is by no means trivial. Indeed it has not been proved so far that such a solution always exists and is stable. In fact, as the discharge is turned on, the joule heating will change the density and the velocity of the flowing medium, which in turn will affect the nature of the discharge by altering the ion and electron mobilities. A mechanism for the raising of instabilities is therefore present. In the following, we shall make the a priori assumption of a stable solution and shall investigate its characteristics. The governing equations† for the discharge are

$$\nabla \cdot (n_i v_i) = S \tag{1}$$

$$\nabla \cdot (n_e v_e) = S \tag{2}$$

where ϕ is the electric potential; $E = -\nabla\phi$ (E being the electric field); $n_i n_e$ are the ion and electron number densities; v_i, v_e are the ion and electron velocities; and S is the source term, number of electrons (ions) generated per unit time and unit volume. Expressions for v_i and v_e are obtained from an approximate solution of the momentum equation for ions and electrons, respectively.

The momentum equation for steady state, in the absence of magnetic fields, reads[5]

$$v_n^{(s)} \frac{\partial v_m^{(s)}}{\partial x_n} + \frac{1}{n^{(s)} m^{(s)}} \frac{\partial \psi_{nm}}{\partial x_m} - \frac{q^{(s)}}{m^{(s)}} E_m = \nu_{sN} (v_m^N - v_m^{(s)}) - \frac{v_m^{(s)}}{n^{(s)}} S^{(s)}$$

where

x_n = x, y_2
$v_m^{(s)}$ = component of velocity of the sth species (ion $s=i$, electron $s=e$) along the mth axis
$m^{(s)}, n^{(s)}$ = atomic mass and number of density, respectively, of the sth species
ν_{sN} = collision frequency between the neutrals and the sth species
$q^{(s)}$ = electrical charge of the sth species
$\psi_{mn}^{(s)}$ = pressure tensor
$S^{(s)}$ = source term of the sth species
v_m^N = component of the neutral flow velocity along the mth axis

We imply summation over repeated indices.

For an approximate solution of the momentum equation, we shall neglect the inertial term and the source terms $S^{(s)}$. For the last assumption, see the discussion in Ref. 6. The pressure tensor can be written as

$$\psi_{mn}^{(s)} = n^{(s)} k T^{(s)} \delta_{mn}$$

where $T^{(s)}$ is the temperature of the specie s assumed to be a constant through the discharge. With these simplifications,

Received Oct. 17, 1977; revision received Feb. 13, 1978.

Index categories: Computational Methods; Plasma Dynamics and MHD.

*Senior Staff Engineer; presently at Hughes Aircraft Company, Culver City, Calif. Member AIAA.

†Gaussian units are used in this paper unless otherwise specified.

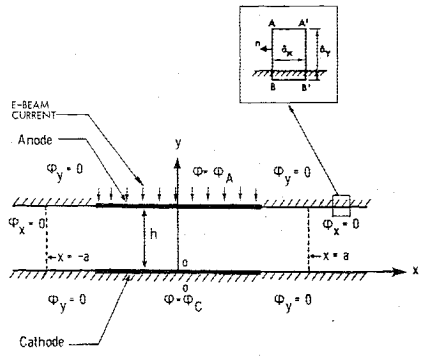

Fig. 1 Discharge and flow geometry.

the momentum equation reduces to

$$n^{(s)} v_m^{(s)} = -\frac{kT^{(s)}}{m^{(s)} \nu_{sN}} + \frac{n^{(s)} q^{(s)}}{m^{(s)} \nu_{sN}} E_m + n^{(s)} v_m^N \tag{3}$$

Let us now define the mobility μ_s and the diffusion coefficient D_s as

$$\mu_s = Nq^{(s)}/m^{(s)} \nu_{sN}, \quad D_s = kT^{(s)}/m^{(s)} \nu_{sN} \tag{4}$$

where N is the neutral particle number of density.

Upon substitution of μ_s and D_s into Eq. (3), we obtain the following vector formulas for the ion drift velocity v_i and electron drift velocity v_e:

$$n_i v_i = n_i[\mu_i(-\nabla\phi/N) + v_f] - D_i \nabla n_i \tag{5}$$

$$n_e v_e = n_e[\mu_e(\nabla\phi/N) + v_f] - D_e \nabla n_e \tag{6}$$

where v_f is the neutral gas-directed velocity.

In the main body of the discharge $n_e \simeq n_i$, typically $|(n_e/n_i) - 1| \simeq 10^{-5}$. We therefore shall assume quasi-neutrality in the rest of this paper, that is, $n_i = n_e \equiv n$. Taking advantage of the quasineutrality assumption, $n_e \simeq n_i$, and subtracting Eq. (1) from Eq. (2), we obtain

$$\nabla \cdot (n_e v_e) - \nabla \cdot (n_i v_i) = 0 \tag{7}$$

Upon substitution of Eqs. (5) and (6) into Eq. (7), we find

$$\nabla n \cdot \left[\frac{\nabla\phi}{N}(\mu_e + \mu_i)\right] + n\nabla\phi \cdot \left[\nabla\left(\frac{\mu_e}{N}\right) + \nabla\left(\frac{\mu_i}{N}\right)\right]$$

$$+ \left(\frac{\mu_i}{N} + \frac{\mu_e}{N}\right)\nabla^2\phi - (D_e - D_i)\nabla^2 n = 0 \tag{8}$$

From both experimental and theoretical considerations, it is well known that $\mu_e \gg \mu_i$. Also,

$$\nabla\mu_{e,i} = \frac{d\mu_{e,i}}{d|\nabla\phi|}\nabla|\nabla\phi|, \quad \frac{d\mu_e}{d|\nabla\phi|} \gg \frac{d\mu_i}{d|\nabla\phi|}$$

Hence, Eq. (8) reduces to the simpler form

$$\nabla \cdot [\mu_e(n/N)\nabla\phi - D_e \nabla n] = 0 \tag{9}$$

We not observe that the second term of Eq. (9) is much smaller than the first term, in the regions of interest of the discharge, and it therefore can be neglected. In fact,

$$n\mu_e(\nabla\phi/N) - D_e\nabla n = n\mu_e(\nabla\phi/N)(1-\epsilon)$$

with

$$\epsilon = \frac{D_e}{\mu_e}\frac{N}{|\nabla\phi|}\frac{|\nabla n|}{n} = \frac{kT}{e|\nabla\phi|}\frac{|\nabla n|}{n}$$

where we used Eq. (4).

It is a simple matter to show that ϵ is always much smaller than unity. In fact, $\Delta n/n$ never greatly exceeds unity, as can be seen from Figs. 2 and 3. Therefore, in order for ϵ to be comparable to unity, we require that $e\nabla\phi \sim kT$; this calls for extremely weak fields, which can be found only on the fringes of the discharge. Therefore, neglecting the diffusion term will only impair the calculations of the weak fringing fields, which can hardly influence the results in the strong field regions, with which we are primarily concerned. An estimate of ϵ between the two electrodes for the typical values of $\nabla\phi \sim \phi_A - \phi_c = 10$, and ambient temperatures considered in this paper, gives

$$\epsilon \simeq 5 \times 10^{-5}(\Delta n/n)$$

We therefore can replace Eq. (9) safely by

$$\nabla \cdot [\mu_e(n/N)\nabla\phi] = 0 \tag{10}$$

Some finer points about the derivation of Eq. (10) now must be made. In fact, at first sight, Eq. (10) is not compatible with the quasineutrality assumption, which implies $\nabla^2\phi = 0$ for $n_i = n_e$, whereas Eq. (10) gives $\nabla^2\phi \neq 0$. Equation (10) was derived from Eqs. (1) and (2) with the quasineutrality and drift velocity assumptions. The quasineutrality assumption must not be understood as $n_i = n_e$ because, were this the case, we could infer that $\nabla^2\phi = 0$. This result would imply that the potential field between the two electrodes is just the vacuum field. It is the small charge separation $|(n_e/n_i) - 1| \simeq 10^{-5}$

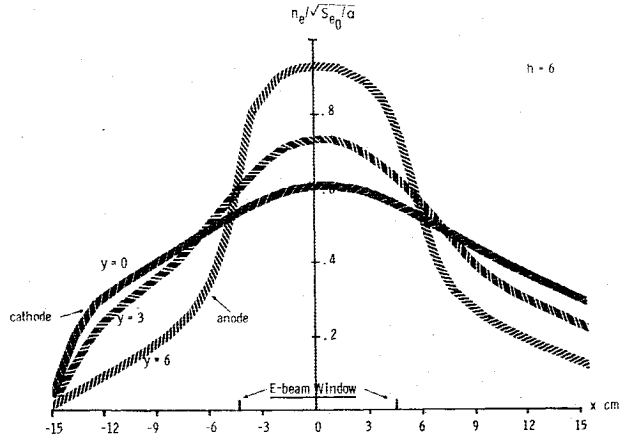

Fig. 2 Normalized electron density as a function of x and y for $\lambda = 0.597$.

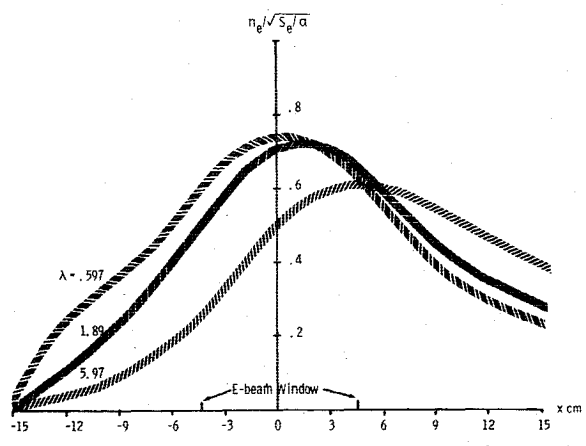

Fig. 3 Normalized electron density as a function of x and λ for $y = 3.0$, channel £.

which skews the vacuum field to preserve the current continuity. There is, therefore, no intrinsic contradiction between Eq. (10) and the quasineutrality assumption.

If we now substitute Eq. (6) into Eq. (2) and use Eq. (9), we obtain the following equation for the charged particle number density:

$$\nabla \cdot (n_e v_f) = S \tag{11}$$

Equations (10) and (11) constitute a self-consistent system, which gives the charged particle density and the electric potential, once the source term $S = S(x,y|\nabla\phi|)$ and the boundary conditions for ϕ and n are prescribed. S is, in general, a function of the field strength $|\nabla\phi|$; for the condition of interest in this paper, however, the dependence of S on the field is weak enough to be neglected.

Observe that Eqs. (10) and (11) are now decoupled, so that the number density for the charged particles can be computed separately from the sustainer field. The only information required is the flow velocity $v_f(x,y)$ and the source term $S(x,y)$ as a function of the position.

In order to be able to integrate Eqs. (10) and (11), boundary conditions must be prescribed. For Eq. (10), the obvious boundary conditions are shown in Fig. 1. The potential ϕ is prescribed on the electrode surfaces. The boundary condition in proximity of the nonconducting channel walls is $\partial\phi/\partial y = 0$. This condition is justified easily as follows. Applying the current conservation equation $\nabla \cdot (n_i v_i - n_e v_e) = 0$ to the "pill box" $AA'B'B$ shown in the inset of Fig. 1, we obtain

$$\int_S \nabla \cdot (n_i v_i - n_e v_e)\,dS = \oint (n_i v_i - n_e v_e) \cdot n\,dl = 0$$

The contributions to the line integral from the two sides AB and $A'B'$ of the "pill box" cancel out in the limit of $\delta x \to 0$. There is no contribution from the side BB', because of the zero conductivity of the wall. The line integral then reduces to

$$\int_{AA'} (n_i v_i - n_e v_e) \cdot n\,dl = 0$$

Let us now take $\delta y \simeq \lambda_e$, where λ_e is the Debye length. For our conditions $\lambda_e \simeq 10^{-4}$ cm. The quasineutrality condition then can be used along AA', and so we find

$$0 = n(v_i - v_e) \cdot n\delta x = \frac{n}{N}(\mu_e - \mu_i)\left(\frac{\partial\phi}{\partial y}\right)_{y=\lambda_e}$$

Hence $(\partial\phi/\partial y)_{y=\lambda e} = 0$. Because of the smallness of λ_e, we shall use, in our calculations $(\partial\phi/\partial y)_{y\simeq 0} = 0$. At $x = \pm a$, we choose to set $\partial\phi/\partial x = 0$. This boundary condition has no physical justification, but it is not expected to change the potential field calculations significantly if a is taken sufficiently large.

The boundary condition for Eq. (11) will be taken as $n_e(x = -a) = 0$. The source term S in Eq. (11) is taken as

$$S = S_E - \alpha n_e^2 \tag{12}$$

where S_E is the e-beam source term, the number of ions (electrons) generated per unit volume and unit time; α is the recombination coefficient, assumed to be constant.

Equation (12) is a very simplified form for S, where charge transfer, attachment, etc., have been neglected. We, however, believe that Eq. (12) still will be sufficient to bring out the major features of the problem. To compute S_E, numerical method employing a Monte Carlo technique currently are used to calculate the trajectories and energy loss of the e-beam electrons.

In this paper only, for purposes of exemplification, a simplified approach[7] for the evaluation of S will be used. For the convenience of the reader, we now shall report the main results of Ref. 7. S_E is given by

$$S_E = \frac{\eta}{e}\frac{dE}{dY} J_{eb}\rho \tag{13}$$

where η is the number of secondary electrons produced per kiloelectron volt deposited in the gas, usually $25 \le \eta \le 29$; e is the electronic charge (C); J_{eb} is the e-beam current density (A/cm^2); ρ is the gas density (mg/cm^3); and $Y = y\rho$. Also

$$\frac{dE}{dY}(x,y) = F(A)\psi(x,y)\frac{dE}{dY}(Y) \tag{14}$$

where the adjustment function

$$F(A) = \left[1 - \frac{\mathcal{E}}{18}\right]\left(0.95 - 0.05\left[\frac{E_0 - 150}{50}\right] + \frac{\mathcal{E}}{10a}\left\{1 + \left[\frac{E_0 - 150}{50}\right]\right\}\right) \tag{15}$$

E_0 is the primary electron energy (keV), and

$$\mathcal{E} = -0.3(\phi_A - \phi_c)/h$$

$$Y_f = Y_{(\text{foil})_{\text{actual}}} + 1.5 + 1.63 \times 10^{-6} E_0^3 \quad \text{(keV)}$$

$$\psi(x,y) = \frac{1}{\pi}\left\{\cos^{-1}\left[\frac{x - \bar{a}}{\sqrt{(x-\bar{a})^2 + (y-h)^2}}\right] - \cos^{-1}\left[\frac{x + \bar{a}}{\sqrt{(x+\bar{a})^2 + (y-h)^2}}\right]\right\} \tag{16}$$

where $\bar{a}$ is the half-width of the e-beam window, and h is the channel height. The e-beam window has been assumed to be located by $y = h$;

$$\frac{dE}{dY}(Y) = [0.78 - 0.005E_0]\left[\frac{E_0}{R_e}\right]\left(1 + \sin\left\{1.29\pi\left[\frac{Y_f + Y}{R_e}\right]\right\}\right) \tag{17}$$

and $R_e = 0.00753E_0^{1.661}$. This formulation for S_e approximates the more accurate Monte Carlo calculations to within 15 to 20%.

A comment on the validity of the results of Ref. 7 for our case now will be made. In Ref. 7, the source term S_e has been derived, accounting for the presence of an accelerating field, which enhances the energy of the primary ionizing electrons as they move along the field. The theory of Ref. 7 has been matched to the results of Monte Carlo calculations, accounting for an accelerating field, by means of a "fudge" factor $F = \frac{1}{2}$; see Eq. (3) of Ref. 7. The general form of Eq. (3) of Ref. 7 obviously can be used also for a decelerating field; the factor F could, in principle, be different. We chose, in the first approximation, to use the same factor $F = \frac{1}{2}$ because of the very small effect that the applied electric field has on the magnitude of the source term S_e in the case under consideration.

Calculation of the Electron Density Distribution

For the electric field calculations, we need to compute $n_e(x,y)$. The gas flows between the two parallel electrodes at velocity $V_f(y)$ directed along the x axis. An e-beam window is placed at $y = h$ between $-\bar{a} \le x \le \bar{a}$. We wish to determine the charged particle distribution under these circumstances.

Under these conditions, Eq. (11) reduces to

$$\frac{d\eta}{dx} + \frac{1}{\lambda}\left(\eta^2 - \frac{S_E}{S_{E_0}}\right) = 0 \tag{18}$$

where

$$\eta = n/n_0 = n/\sqrt{S_{E_0}/\alpha}$$

$$\lambda = v_f(y)/\sqrt{\alpha S_{E_0}} \quad \text{(dimension of a length)}$$

$$S_{E_0} = S_E(-a \le x \le a, \quad y = h)$$

Equation (18) can be integrated numerically if S_E/S_{E_0} and $\eta(x=0)$ are given. The results of the numerical integration are shown in Figs. 2 and 3. S_E/S_{E_0} was computed using Eqs. (13-17); the parameter λ, which characterizes the shape of the charged particle distribution, was taken as $\lambda = 0.597$, 1.89, and 5.97. This corresponds to e-beam current densities of 10^{-2}, 10^{-3}, and 10^{-4} A/cm^2, respectively, when α is taken as 10^{-7} cm^3-s^{-1}, $V_f(y=h/2) = 6.65 \times 10^4$ cm/s, and $E_0 = 150$ keV. These conditions correspond to the ones generally encountered in a variety of gas lasers. The channel height was taken to be 6 cm, and $\bar{a} = 4.5$ cm. In Fig. 2, the normalized electron density is shown for different values of y. As can be seen from Fig. 3, large values of λ skew the charged particles distribution downstream.

A large value of λ corresponds to high flow velocities combined with low generation of recombination rates. For stationary flow, Eq. (11) reduces to $S = 0$, and from Eq. (12) we immediately find $n_e = \sqrt{S_E/\alpha}$. The skewing of the charged particle distribution will, in turn, distort the electric field of the cavity, as will be shown in the following sections.

Calculation of the Potential Field Between the Electrodes

Once the electron density has been evaluated and the density of neutral particles $N(x,y)$ is known, Eq. (8) can be integrated numerically with the boundary conditions shown in Fig. 1. For the purpose of solving Eq. (8) in a two-dimensional rectangular domain, a numerical code was developed for the integration of the elliptical second-order equation of the form

$$\nabla^2\phi(x,y) + a_x(x,y)\frac{\partial\phi}{\partial y} + a_y(x,y)\frac{\partial\phi}{\partial y} = 0$$

where a_x, a_y are assigned variable coefficients. The code can handle Dirichlet, Neumann, or mixed boundary conditions.

The code was developed with the flexibility of using a variable mesh size in both the x and y directions. This capability was required in order to handle the transition regions at the cathode and anode edges. In these regions, where the boundary conditions change abruptly from Dirichlet to Neumann or vice versa, large fields are developed over very short distances, and therefore a much finer mesh size is required than in the other regions of the discharge. This variable mesh size capability offers a large savings on the total number of points in the mesh, and therefore a savings in computer core requirement and in computing time. The finite-difference equations derived from Eq. (10) were solved using the standard successive overrelaxation method.[8]

The typical case of our calculations is characterized by the following parameters:

a = 15 cm
h = 6 cm, channel height
$\phi_A = 5$ statV, $\phi_C = -5$ statV, anode and cathode potentials
$\alpha = 10^{-7}$ cm^3/s, recombination coefficient
$\mu_e = 4 \times 10^{24}$ cm^{-3}/g$^{-1/2}$ electron mobility; for N_2, the electron mobility was taken as a constant for simplicity in our test case; the program is, however, capable of handling the electron mobility as a function of the strength of the field, provided that the proper dependence is supplied. $J_{eb} = 10^{-2}$, 10^{-3}, 10^{-4} A/cm^2, e-beam current

Boundary layers are developed along the side walls of flowing gas lasers. Steep density gradients are generated both by the flow, if it has a large Mach number as in a supersonic CO laser, and/or in conjunction with the cathode and anode falls, where large amounts of heat are dissipated.

From the calculations of Refs. 6 and 9, we can describe approximately the density and velocity variations in proximity of the cathode and anode in the following way:

$$N(x,y) = 2.58 \times 10^{17}\,\text{cm}^{-3} \text{ for } 0.6 \le y \le 5.4, \; -\infty < x < \infty$$

$$N(x,y) = 2.58 \times 10^{17}(0.1 + 1.5y)\,\text{cm}^{-3} \text{ for } 0 \le y \le 0.6, \; -\infty < x < \infty$$

$$N(x,y) = 2.58 \times 10^{17}[1 - 1.5(y - 5.4)]\,\text{cm}^{-3} \text{ for } 5.4 \le y \le 6, \; -\infty < x < \infty$$

$$[V_f(x,y)]_x = 6.65 \times 10^4\,\text{cm/s} \text{ for } 0.6 \le y \le 5.4, \; -\infty < x < \infty$$

$$[V_f(x,y)]_x = 1.108 \times 10^5 y\,\text{cm/s} \text{ for } 0 \le y \le 0.6, \; -\infty < x < \infty$$

$$[V_f(x,y)]_x = 6.65 \times 10^4[1 - 1.66(y - 5.4)]\,\text{cm/s} \text{ for } 5.4 \le y \le 6, \; -\infty < x < \infty$$

$$[V_f(x,y)]_y = 0 \text{ for } 0 \le y \le 6, \; -\infty < x < \infty$$

The neutral density $N(x,y)$ and flow velocity $V_f(x,y)$ have been assumed constant in the bulk of the discharge. The results of our calculations then will represent only a first-order solution, inasmuch as the joule heating effects on $N(x,y)$ and $V_f(x,y)$ have been neglected, except for the cathode and anode fall regions, where they are most severe.

The results of the present numerical calculations now will be examined in some detail. The chosen mesh size was $\Delta x = 1.0$ cm and $\Delta y = 0.6$ cm. A smaller mesh size was utilized in the proximity of the cathode and anode to account for the more rapid change of the fields due to the variation in the neutral densities. Five mesh points were inserted between two neighboring mesh points in a geometrical progression fashion, starting with the smallest interval at the wall. In a similar way, mesh points were inserted in the region of transition of the boundary conditions. Figure 4 shows the effect of the insertion of points at the transition regions on the current density. The upstream and downstream edges of the cathode and anode are located at $x = \mp 5$ cm. The total number of points in x, inserted at -6 cm $\le x \le -4$ cm and 4 cm $\le x \le 6$ cm, is $2n$. Figure 4 shows that, as n is increased, that is, as more points are added, the current peak at the cathode edge moves closer to the beginning of the metal and becomes larger in absolute value. This clearly signals the presence of a singularity. However, the exact location of the singularity, as can be seen from Fig. 4, does not affect sensibly the overall current density distribution over the cathode. Moreover, the total current is hardly affected by a change in n for $n \ge 5$. We therefore choose for our calculations $n = 5$.

Note that the presence of the singularity is due only to our modeling of the transition region between the conducting and nonconducting walls. The abrupt change of boundary conditions forces the field to reach an infinite value. In a real physical situation, a charge distribution will be established which would prevent the appearance of the singularity, which would be replaced by strong but finite fields. Our quasineutrality assumption does not allow us to examine the detail of the transition region.

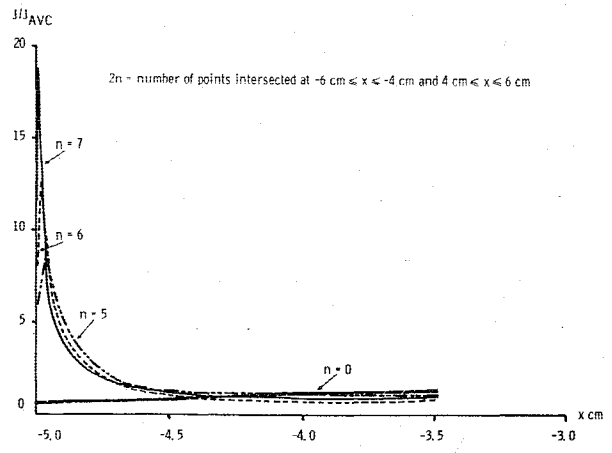

Fig. 4 Details of current density calculations in the upstream corner of the cathode ($\lambda = 0$).

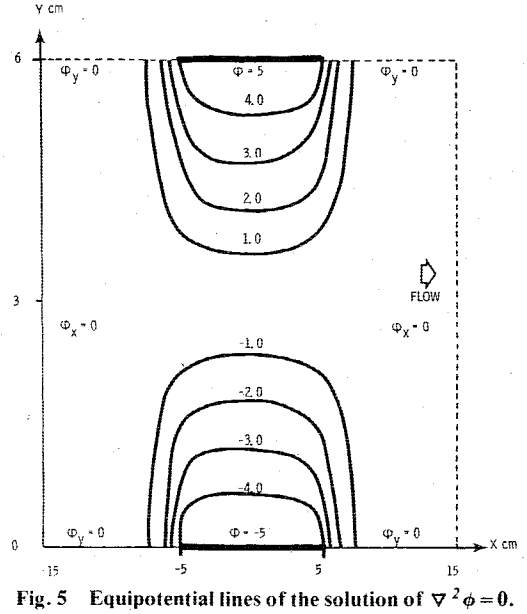

Fig. 5 Equipotential lines of the solution of $\nabla^2\phi = 0$.

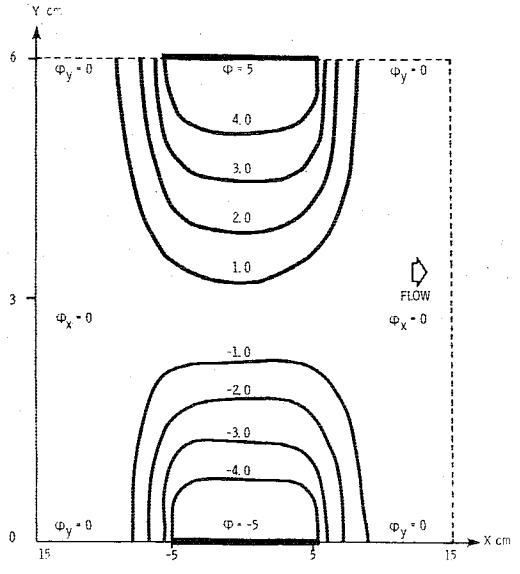

Fig. 6 Equipotential contours for $\lambda = 0$.

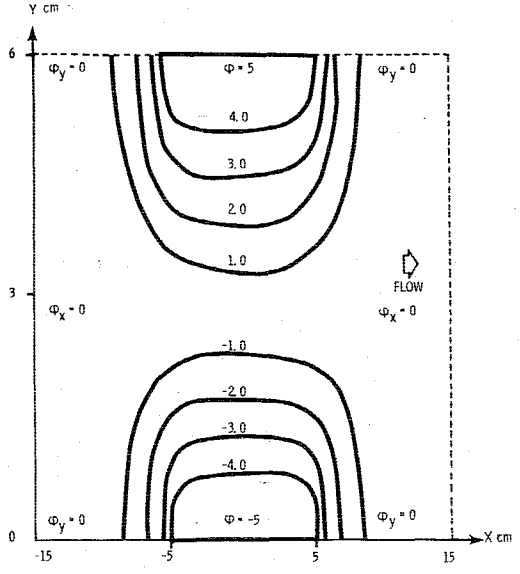

Fig. 7 Equipotential contours for $\lambda = 0.597$.

In Fig. 5, we show the equipotential lines for the solution of the Laplace equation, $\nabla^2\phi = 0$, corresponding to the case with no conducting medium between the electrodes. The boundary conditions employed are shown on the figure. The positions of the vertical boundaries were chosen at $x = \pm 15$ cm. Some test cases were run with the vertical boundaries located at $x = \mp 30$ cm; no noticeable change in the final results was detected. The irregularities in the plotted curves reflect the inaccuracies of the "printer plot" utilized in producing the graphs.

In Figs. 6-9, the equipotential contours for $\lambda(y = h/2) = 0$, 0.597, 1.88, and 5.97 are shown. We can notice a flattening of the potential slope in the upstream direction for increasing values of λ, along both the cathode and the anode. Similarly, a smaller steepening of the potential hill along the cathod and the anode can be observed in the downstream direction. This phenomenon can be related to the larger electron accumulation in the downstream regions of the cavity, as shown in Fig. 3. For increasing values of λ, more electrons are carried downstream, and larger electric fields in the x direction are generated in proximity of the downstream edge of the cathode and anode. The opposite happens at the upstream edges.

In Fig. 10, we plot the normalized component of the electric field in the y direction as a function of y at $x = 0$ for different values of λ. The electric field has been normalized to the constant strength of the field with no conducting medium. From Fig. 10, we note that the electric field strength is not affected strongly by the value of λ. In the proximity of the cathode, the field is larger than in the proximity of the anode. This is in agreement with the fact that, in our configuration of an e-beam window at the anode, larger electron densities are found at the anode than at the cathode. The steep drop of the fields at both the cathode and anode is related to the assumed decrease of the neutral density in the proximity of the wall.

In Fig. 11, the effects of the neutral density variations through the boundary layer and of V_f on E_y/E_{y0} are shown. The drop in the magnitude of E_y/E_{y0} at the cathode and anode is removed if constant density all across the cavity is assumed. The effect of assuming $V_f \neq$ const in proximity of the cathode and anode is negligible.

In Fig. 12, the normalized current density on the surface of the cathode is shown for different values of the parameter λ. For all three values of λ considered, the current density in the downstream region of the cathode is higher than that in the upstream part. Again, this relates to the higher electron accumulation in the downstream areas of the cavity. This is in qualitative agreement with the experimental findings of Ref. 4.

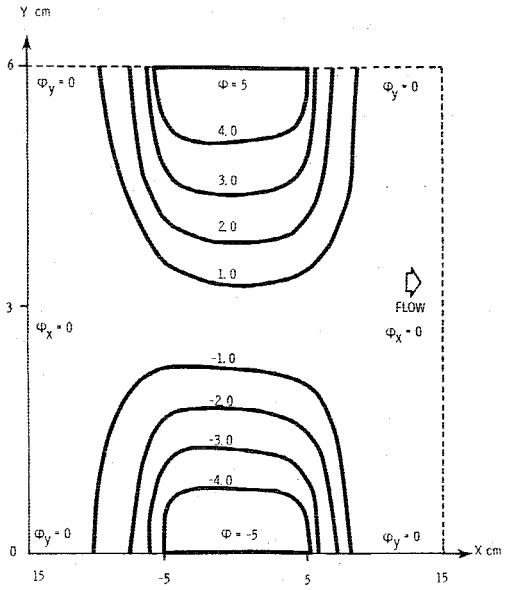

Fig. 8 Equipotential contours for $\lambda = 1.88$.

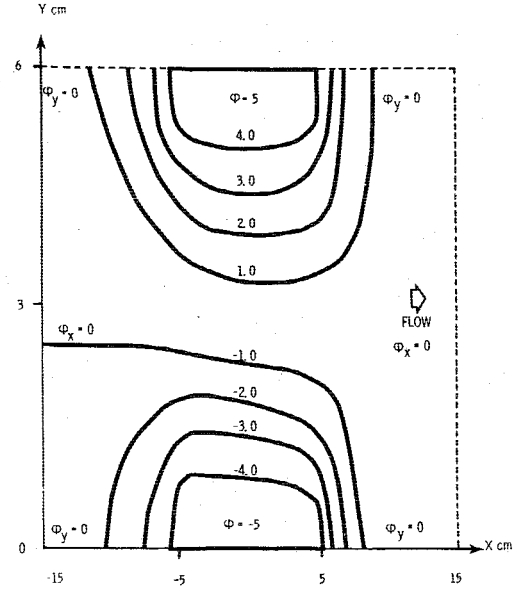

Fig. 9 Equipotential contours for $\lambda = 5.97$.

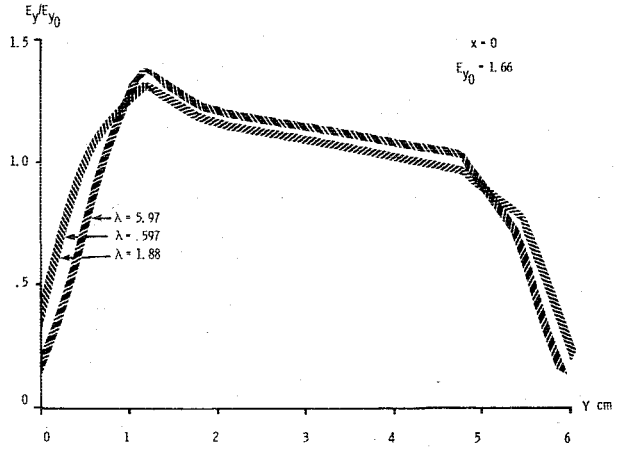

Fig. 10 Normalized electric field in the Y direction as a function of Y for different values of the parameter λ.

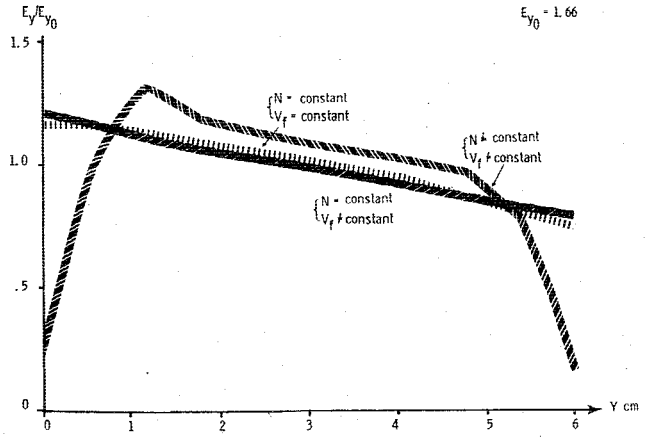

Fig. 11 Normalized electric field in the Y direction as a function of Y.

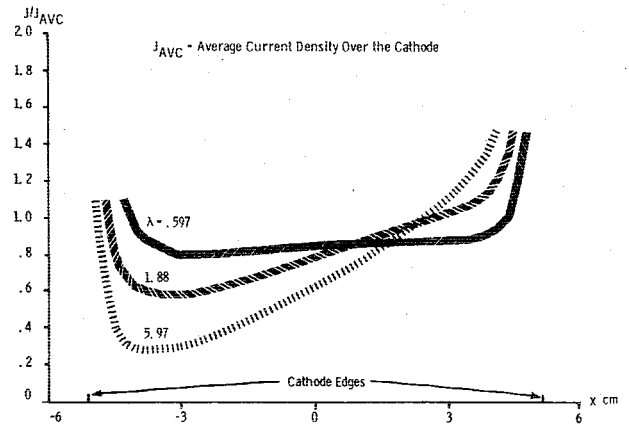

Fig. 12 Normalized current density over the cathode for different values of $\lambda = V_f/\sqrt{S_{E_0}\alpha}$.

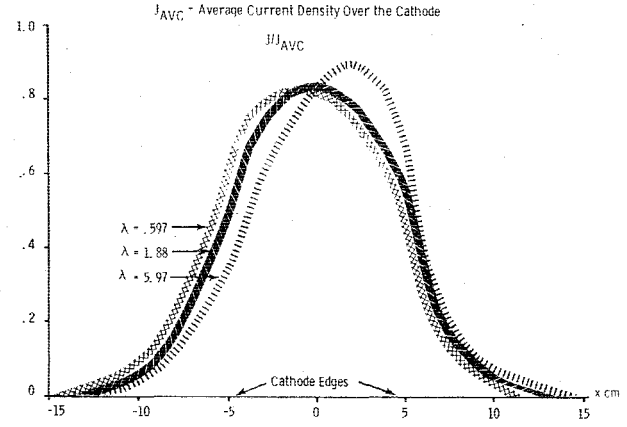

Fig. 13 Normalized current density at midplane for different values of λ.

In Fig. 13, the normalized current density at the midplane between anode and cathode is shown for different values of λ. The current distribution is skewed in the downstream direction for large values of λ, as expected, because of the skewing of the electron density distributions. The current density distributions shown in Fig. 13 also explain the strengthening of the x component of the electric field in the downstream direction for increasing values of λ. The opposite applies to the upstream direction.

Figures 14-16 show the constant-power deposition contours for different values of λ. As the value of λ is increased, we

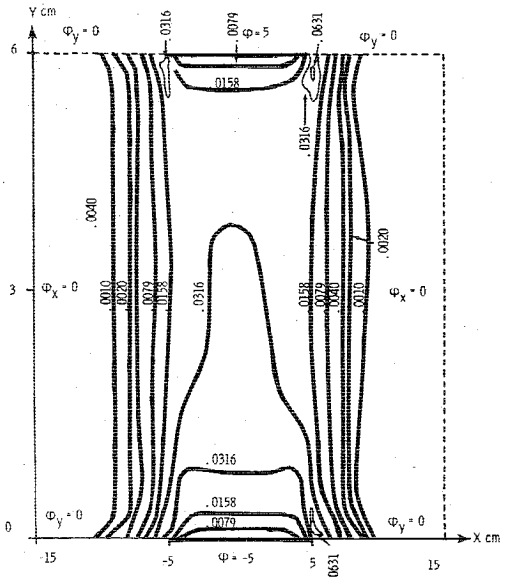

Fig. 14 Constant-power deposition contours for $\lambda = 0.597$; the normalization factor is the peak power of 6.05×10^{11} ergs/cm^3-s at $x = -5, y = 0.02$.

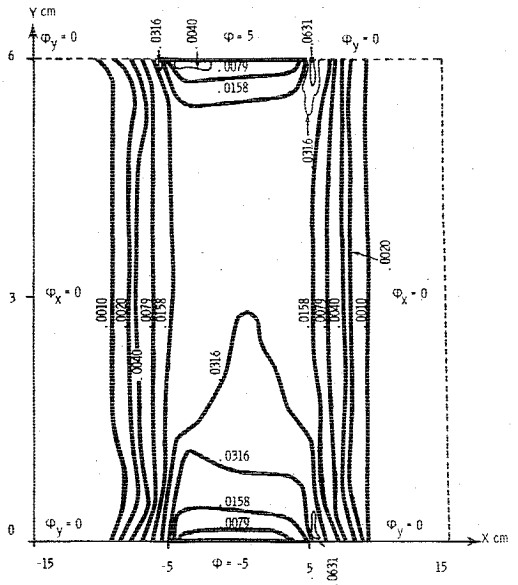

Fig. 15 Constant-power deposition contours for $\lambda = 1.88$; the normalization factor is the peak power of 2.0×10^{11} ergs/cm^3-s at $x = 5.03, y = 0.02$.

again note a downstream steepening of the power contours. The most obvious changes are found in the 0.0316 power contours, which shrink closer to the cathode as λ is increased. The most marked changes are found between $\lambda = 1.88$ and $\lambda = 5.97$. As indicated in Figs. 14-16 peaks in the power deposition occur in the proximity of the electrode edges. This is consistent with the fact that electric field singularities are present at the edges of the electrodes. The absolute magnitude of these peaks is only indicative of the real power deposition, because of the limited accuracy of the numerical and physical models in the presence of very high electric fields; however, the existence of high-power deposition in the proximity of the electrode edges is indicated clearly. Finally, in Fig. 17, the average cathode current J_{AVC} is plotted against J_{eb}. Note that the square-root law is followed at higher e-beam currents, but deviations occur at lower values of J_{eb}.

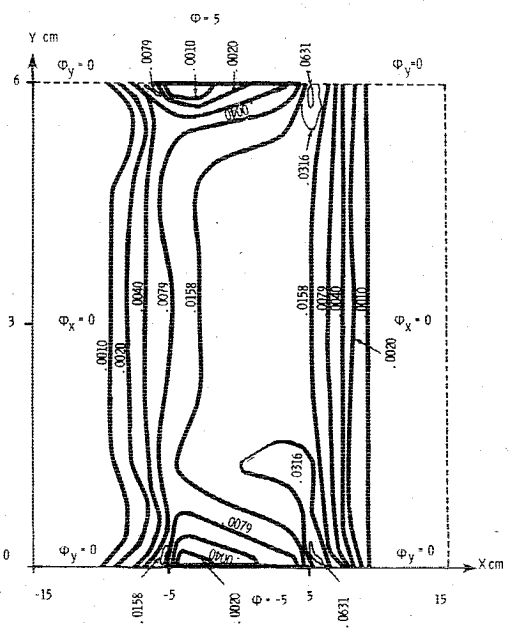

Fig. 16 Constant-power deposition contours for $\lambda = 5.97$; the normalization factor is the peak power of 6.57×10^{10} ergs/cm^3-s at $x = 5.03, y = 0.02$.

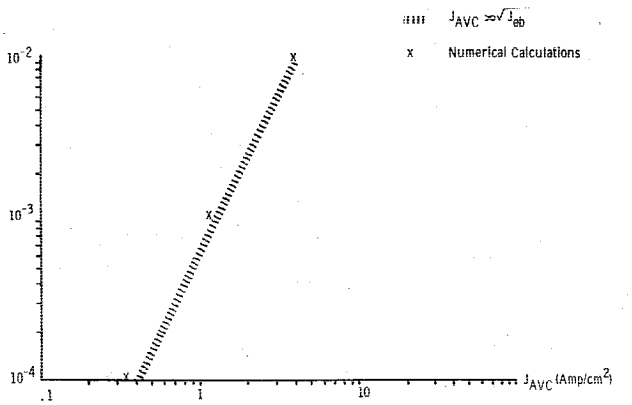

Fig. 17 Average current density on the cathode as a function of the e-beam current density.

Summary and Conclusions

A numerical method for the calculation of the power deposition in an e-beam stabilized discharge has been developed. Allowance has been made for the effect of the flowing gas. The results of a few typical calculations show that the nonuniformity in the electron densities, coupled with the neutral drift and neutral density variations, can substantially change the results that would be expected using a vacuum field approximation. The code can be applied under a variety of conditions in a rectangular domain. No feedback from the joule heating of the gas has been included.

Acknowledgments

The support of B. B. O'Brien Jr. and M. J. Plummer, whose discussion and criticisms were essential to the development of this work, is sincerely appreciated. Also, a special thanks goes to Gordon Duckworth for his invaluable help with the computer programming and to Renée G. Moore for her technical assistance.

References

[1] Reilly, J. P., "Pulsar/Sustainer Electric-Discharge Laser," *Journal of Applied Physics*, Vol. 43, Aug. 1972, pp. 3411-3416.

[2] Jacob, J. H., Reilly, J. P., and Pugh, E. R., "Electron-Beam Spreading and its Effect on Sustainer Current and Field Distribution in CO_2 Lasers," *Journal of Applied Physics*, Vol. 45, June 1974, pp. 2609-2613.

[3] Theophanis, V. A., Jacob, J. H., and Sackett, S. J., "Discharge Spatial Nonuniformity in *E*-Beam-Sustainer CO_2 Lasers," *Journal of Applied Physics*, Vol. 46, May 1975, pp. 2329-2331.

[4] "Supersonic Continous Wave CO Electric Discharge Laser Parametric Investigation," Mathematical Science Northwest, Inc., Belevue, Wash., AFWL-TR-76-298, 1976.

[5] Holt, E. H. and Haskell, R. E., *Foundations of Plasma Dynamics*, 1st ed., Macmillan, New York, 1965, p. 162.

[6] Parazzoli, C. G., "Turbulent Boundary Layer Over the Cathode of a High Current Discharge: Numerical Calculation and Experimental Results," Northrop Research and Technology Center, NRTC-76-31R, June 1976.

[7] Cason, C., Perkins, J. F., and Werkheiser, A. H., "*E*-Beam Spreading and Resulting Plasma Variation in CO_2 Laser Plasmas," AIAA Paper 77-65, 1977.

[8] Ames, W. F., *Numerical Methods for Partial Differential Equations*, 2nd ed., Academic Press, New York, 1977, p. 119.

[9] Parazzoli, C. G., "Boundary Layer in a High Current Density Discharge," *AIAA Journal*, Vol. 15, June 1977, pp. 849-853.